NANOSYSTEMS:
PHYSICS, CHEMISTRY, MATHEMATICS

Smal E., et al. *Nanosystems: Phys. Chem. Math.*, 2024, **15** (6), 879–892.
http://nanojournal.ifmo.ru
DOI 10.17586/2220-8054-2024-15-6-879-892

Original article

Chemical looping methane dry reforming over Ni-containing modified ceria-zirconia

Ekaterina Smal[1,a], Valeria Fedorova[1,b], Konstantin Valeev[1,c], Amir Hassan[2,d], Evgeny Gerasimov[1,e], Mikhail Simonov[1,f]

[1]Boreskov Institute of Catalysis SB RAS, Novosibirsk, Russia
[2]Novosibirsk State University, Novosibirsk, Russia

[a]smal@catalysis.ru, [b]valeria@catalysis.ru, [c]valeev@catalysis.ru, [d]a.khassan1@g.nsu.ru, [e]gerasimov@catalysis.ru, [f]smike@catalysis.ru

Corresponding author: Ekaterina Smal, smal@catalysis.ru

PACS 61.46.+w, 82.40.-g, 82.65.+r

ABSTRACT Modified ceria-zirconia oxides were prepared in supercritical fluids in flow-type installation. Ni was added by wetness impregnation. All materials were studied by a complex of physicochemical techniques (XRD, TEM, H_2-TPR). Catalysts have been investigated in a modern process – chemical looping methane dry reforming (CLMDR). Conversions of CH_4 and CO_2, H_2/CO ratio, H_2 and CO productivities were calculated. The features of CLMDR process were compared with results obtained in MDR steady-state conditions.

KEYWORDS chemical looping, methane dry reforming, hydrogen, ceria-zirconia, supercritical synthesis

ACKNOWLEDGEMENTS This work was supported by the Ministry of Science and Higher Education of the Russian Federation within the governmental assignment for Boreskov Institute of Catalysis (project FWUR-2024-0033).
The studies were carried out using the facilities of the shared research center "National Center of Investigation of Catalysts" at Boreskov Institute of Catalysis.
Authors thank to T. Krieger and O. Bulavchenko for XRD, V. Rogov for H_2-TPR and A. Ishchenko for TEM studies.

FOR CITATION Smal E., Fedorova V., Valeev K., Hassan A., Gerasimov E., Simonov M. Chemical looping methane dry reforming over Ni-containing modified ceria-zirconia. *Nanosystems: Phys. Chem. Math.*, 2024, **15** (6), 879–892.

1. Introduction

Methane dry reforming process (MDR) (1) is a route to utilize and convert two major greenhouse gases – CH_4 and CO_2 – to syngas and hydrogen [1–3]. Syngas can be obtained with a low H_2/CO molar ratio equal to 1, which is suitable for obtaining valuable liquid hydrocarbons through Fischer–Tropsch synthesis [4].

$$CH_4 + CO_2 \rightarrow 2H_2 + 2CO, \quad \Delta H^0_{298\,K} = 247 \text{ kJ/mol}. \tag{1}$$

However, the side reaction of reverse water gas shift (RWGS) (2) caused by the simultaneous presence of CO_2 and hydrogen results to decrease of H_2/CO ratio during MDR [5]. So, it is important to find a way to carry out the MDR reaction in order to exclude the occurrence of RWGS reaction.

$$CO_2 + H_2 \rightleftarrows CO + H_2O, \quad \Delta H^0_{298\,K} = -41 \text{ kJ/mol}. \tag{2}$$

Another problem of conventional MDR is rapid coke formation which occurs due to methane decomposition (3) at low temperatures and CO disproportionation (Boudouard reaction) at high temperatures (4) [6].

Both side reactions lead to active centers blocking and catalyst deactivation.

$$CH_4 \rightarrow C + 2H_2, \quad \Delta H^0_{298\,K} = 75 \text{ kJ/mol}, \tag{3}$$

$$2CO \rightarrow C + CO_2, \quad \Delta H^0_{298\,K} = -171 \text{ kJ/mol}. \tag{4}$$

Chemical looping methane dry reforming process (CLMDR) is the attractive way to resolve both these issues. In this mode, consistent feed of CH_4 and CO_2 is implemented, which eliminates the contribution of RWGS side reaction [7–9].

The first step of CLMDR includes reaction of methane with support reactive oxygen with its partial oxidation and selective production of syngas (5). Further, the reduced support would be re-oxidized by CO_2 to regenerate the reactive oxygen (6). Successive red-ox cycles drive the continuous conversion of CO_2 and methane to syngas with a higher H_2/CO molar ratio. The total process stoichiometrically corresponds to the conventional catalytic MDR although it is divided in time into two independent heterogeneous reactions [7–9].

$$CH_4 + \text{cat}_{\text{Ox}} \rightarrow 2H_2 + CO + \text{cat}_{\text{Red}}, \tag{5}$$

$$CO_2 + \mathrm{cat_{Red}} \rightarrow \mathrm{cat_{Ox}} + CO, \quad (6)$$

$\mathrm{cat_{Ox}}$ = oxidized catalyst and $\mathrm{cat_{Red}}$ = reduced catalyst [8].

Moreover, compared with MDR process, during CLMDR, the carbon generated by CH_4 pyrolysis can be oxidized by CO_2 at the oxidation step, which can reduce the carbon deposition to a certain extent and also produce syngas with adaptable hydrogen/carbon molar ratio [7].

In the literature, catalysts for the chemical looping processes are called oxygen carriers. They consist of reducible metal oxides, which must have the following characteristics: ability to generate oxygen ions or vacancies and electrons or holes, facilitate their diffusion in the bulk phase and provide active sites for surface reactions [10–12].

Another important factor is strength of the surface M–O bonds. If they are too weak, the full oxidation will occur at the reduction stage instead of partial one. However, they should also not be too strong, otherwise the material will be a weak oxidant. An ideal oxygen carrier has intermediate bond strength and mobility of lattice O atoms to drive the process both selectively and kinetically fast. Such materials include oxides with fluorite, perovskite and rocksalt structures, and most of investigated catalysts are based on them [12].

Furthermore, for practical applications these materials should exhibit long-term redox stability, fast reaction kinetics, reasonable oxygen and heat capacity and conductivity, be mechanically and thermally robust under the operation conditions [12].

It is well known that CeO_2 has a good thermal stability and a high oxygen mobility/storage capacity due to its redox couple (Ce^{4+}/Ce^{3+}) being perspective support for high temperature processes such as MDR and CLMDR [7–9, 13, 14]. However, different ways to increase oxygen mobility of CeO_2 oxide are under investigation. For example, ceria modification by zirconium with solid solution formation leads to increased oxygen mobility [15]. Besides, partial replacement of cerium with zirconium in CeO_2 can improve the oxygen storage capacity and catalytic performance in MDR process because of the easy formation of oxygen vacancies [16].

It was shown that Ni-containing catalysts based on ceria-zirconia are attractive for MDR process due to their low price and high activity [13, 17–19]. In recent years, the influence of dopant metals (Ti, Nb, Pr) in ceria or ceria-zirconia on catalytic activity in MDR was investigated by our research group [20–25] and other groups as well [26–29]. Ni-containing catalysts based on Ce–Pr mixed oxide show higher activity in MDR process at 700 °C compared with Ce–Zr-based catalyst [23, 25, 30].

It is well known that the preparation method has a great influence on the properties of the resulting oxides, which consequently affects their interaction with the supported metal component and catalytic activity in the target reaction. There are a lot of various methods for the preparation of mixed Ce–Zr oxides described in the literature: solid-phase synthesis [31], the Pechini method [32], coprecipitation [33], sol-gel technology [34, 35], hydrothermal synthesis [36], solvothermal method [37], microemulsions [38], the microwave method [39], the sonochemical method [40], solution combustion [41] and spray pyrolysis reactions [42].

In recent years, synthesis in supercritical alcohols is of growing interest, since it is characterized by low energy consumption, simple implementation, allows obtaining mixed oxides with high structural homogeneity and affecting their morphology by varying synthesis conditions such as pressure, temperature and nature of supercritical solvent [25, 43]. In our previous study [20], it was shown that synthesis in supercritical isopropanol allows obtaining single-phase mixed Ce–Zr-(Ti/Nb) oxides, in contrast to the Pechini method.

The CLMDR was studied earlier using Ni-containing catalysts based on pure ceria [7–9] only. It was shown in [8] that conversions of CH_4 and CO_2 were equal to 85 % after 12 cycles at 700 °C for initial reaction mixture containing 5 % of CH_4 or CO_2. However, this concentration is too low for practical use. It should be emphasized that CLMDR is a process potentially capable of producing synthesis gas suitable for the synthesis of hydrocarbons, so the design of highly active catalysts is an urgent task.

The objective of the present work is to study the Ni-containing catalysts based on modified ceria-zirconia prepared in supercritical fluids in chemical looping methane dry reforming reaction. The novelty of this work is using namely modified ceria-zirconia as supports in the process of CLMDR. Moreover, in our work, we use more concentrated reaction mixtures containing 15 % of reagents.

$Ni/Ce_{0.75}Zr_{0.25}O_2$, $Ni/Ce_{0.75}Ti_{0.1}Zr_{0.15}O_2$, $Ni/Ce_{0.75}Ti_{0.05}Nb_{0.05}Zr_{0.15}O_2$ and $Ni/Ce_{0.75}Pr_{0.1}Zr_{0.15}O_2$ compositions were earlier investigated as catalysts for conventional MDR process [20, 25] and demonstrated high activity in this reaction. So they were chosen in the present work for further studies as catalysts for CLMDR process. The influence of dopant metals in supports and comparison with results obtained in MDR steady-state conditions are presented.

2. Experimental section

2.1. Preparation of Ni-containing modified ceria-zirconia materials

The modified ceria-zirconia supports were synthesized by the solvothermal method using supercritical conditions in the flow-type reactor [20]. $Ce(NO_3)_3 \cdot 6H_2O$ (pure for analysis, Vecton, Russia), $Zr(OBu)_4$ (80 wt% in n-butanol, Alfa Aesar, Germany), $Ti(OC_4H_9)_4$ (Acros Organics, Belgium), $NbCl_5$ (Acros Organics, Belgium) and $Pr(NO_3)_3 \cdot 6H_2O$

(chemically pure, Krane, Russia) were used as supports precursors. Starting salts were dissolved in isopropanol (particularly pure, Soyuzkhimprom, Russia); only $Zr(OBu)_4$ was dissolved in n-butanol (chemically pure, Komponent-Reaktiv, Russia) with acetylacetonate (pure, Interhim, Russia) as complexing agent. Isopropanol was used as a supercritical alcohol in the synthesis process. The molar concentrations of Ce and Zr were 0.25 and 0.8 – 1 mol/L, respectively. The temperature of oxide synthesis was 400 °C, the pressure in the reaction system was 120 atm, the feed rate of the salts solution was 5 mL/min, and the solvent feed rate was 9 mL/min. After leaving the reactor, the exit stream was depressurized and cooled, and suspension of solid particles in the mother liquid was collected in a storage container. Obtained powders were decanted, dried at 200 °C and calcined at 700 °C during 2 h.

All catalysts were obtained by the incipient wetness impregnation of the supports with water solution of $Ni(NO_3)_2 \cdot 6H_2O$ (pure for analysis, Vecton, Russia) and subsequent drying and calcination at 700 °C during 2 h. Ni amount was 5 wt.% in all samples.

2.2. Catalysts characterization

X-Ray diffraction analysis (XRD) was carried out using a D8 Advance (Bruker, Germany) diffractometer with Cu Kα radiation and LynxEye detector. The XRD pattern was collected in the 2θ range 20 – 85 °C with a 0.05 step size and 3 s accumulation times.

The *in situ* XRD experiment was carried out using XRK-900 high-temperature flow chamber (Anton Paar, Graz, Austria). The sample was placed in a chamber and purged with He flow. Next, the heating of the chamber was turned on (heating rate 12 °C/min). The mixture of H_2 in He (H_2:He = 1:2) was fed at a temperature about 300 °C. The sample was reduced by hydrogen to 700 °C. Then the chamber was purged with He for 0.5 h and flow of pure CO_2 was supplied. The first diffractogram under CO_2 was recorded after 0.5 h, the second one – after 2 h. Then the sample was cooled to a room temperature under He flow. The final diffractogram was recorded after night under air. The lattice parameters were calculated using the least squares method by Polycrystal software [44].

Specific surface area (SSA) was defined by the BET method using a Quadrasorb evo (Quantachrome Instruments, USA) installation.

Reducibility of samples pretreated in O_2 at 500 °C were studied by the temperature programmed reduction by H_2 (H_2-TPR) with the temperature ramp 10 °/min from 60 to 900 °C using 10 % H_2 in Ar mixture and GC Tsvet 500 (Russia).

TEM (transmission electron microscopy) micrographs were obtained with a Themis-Z3.1 instrument (TFS, USA) equipped with X-FEG monochromator and CS/S double corrector, accelerating voltage 200 kV and with a JEM-2200FS transmission electron microscope (JEOL Ltd., Japan, acceleration voltage 200 kV, lattice resolution $\sim$ 1 Å) equipped with a Cs corrector. Elemental analysis was performed with a Super-X EDS detector (energy resolution about 120 eV) in HAADF-STEM mode. Samples for the TEM study were prepared by ultrasonic dispersing in ethanol and subsequent deposition of the suspension upon a "holey" carbon film supported on a copper grid.

2.3. Catalytic Tests

2.3.1. Chemical looping methane dry reforming technique (CLMDR). Before reaction the catalysts were pretreated in 10 vol. % O_2/N_2 at 600 °C for 30 min and then in 5 vol. % H_2/He at 600 °C for 1 h. Chemical looping methane dry reforming process (CLMDR) was carried out at 700 °C under atmospheric pressure in flow-type installation. Contact time was 10 ms. The gas stream was switched periodically between inert gas (He) to one containing 15 vol.% CH_4/He at reduction step and 15 vol.% CO_2/He at oxidation step. Each cycle consists of a reduction step of 1 min, He purge of 2 min, an oxidation step of 1 min, and again He purge of 2 min. Cycles were repeated 12 times.

During the cyclic supply of reagents, the concentrations of products in the reaction mixture were continuously measured using a gas analyzer Test-1 (Boner, Russia). The measured concentrations were recalculated to reagents and products flow (mol·min^{-1}) and integrated over time into the amount of substance in each cycle.

The reagents conversions were calculated as follows:

$$X_{\mathrm{CH_4}}\,(\%) = \frac{\upsilon_0 - \upsilon}{\upsilon_0} \cdot 100\,\%$$

at reduction step,

$$X_{\mathrm{CO_2}}\,(\%) = \frac{\upsilon_0 - \upsilon}{\upsilon_0} \cdot 100\,\%$$

at oxidation step, where υ_0, υ – initial and final reagent amount of substance, respectively (mol).

H_2/CO ratio was calculated both at reduction step and taking into account the total amount of CO produced during each cycle:

$$\frac{\mathrm{H_2}}{\mathrm{CO}}\mathrm{ratio} = \frac{\upsilon(\mathrm{H_2})}{\upsilon(\mathrm{CO})}.$$

H_2 productivity was calculated at reduction step (mol·g^{-1}):

$$Y_{\mathrm{H_2}} = \frac{\upsilon(\mathrm{H_2})}{m_{\mathrm{cat}}}.$$

CO productivity was calculated at reduction and oxidation step (mol·g^{-1}):

$$Y_{\mathrm{CO}} = \frac{v(\mathrm{CO}^R) + v(\mathrm{CO}^O)}{m_{\mathrm{cat}}}.$$

Carbon balances were calculated both separately at each stage and in total at each cycle using the following formulas:

$$\mathrm{CarbonBalance(R)} = \frac{v(\mathrm{CH_4}^{\mathrm{R}})+v(\mathrm{CO_2}^{\mathrm{R}})+v(\mathrm{CO}^{\mathrm{R}})}{v_0(\mathrm{CH_4})} \cdot 100\ \%,$$

$$\mathrm{CarbonBalance(O)} = \frac{v(\mathrm{CO_2}^{\mathrm{O}})+v(\mathrm{CO}^{\mathrm{O}})}{v_0(\mathrm{CO_2})} \cdot 100\ \%,$$

$$\mathrm{CarbonBalance(All)} = \frac{v(\mathrm{CH_4}^{\mathrm{R}})+v(\mathrm{CO_2}^{\mathrm{R}})+v(\mathrm{CO}^{\mathrm{R}})+v(\mathrm{CO_2}^{\mathrm{O}})+v(\mathrm{CO}^{\mathrm{O}})}{v_0(\mathrm{CH_4})+v_0(\mathrm{CO_2})} \cdot 100\ \%.$$

Hydrogen balances was also calculated:

$$\mathrm{HydrogenBalance} = \frac{2 \cdot v(\mathrm{H_2}^R) + 4 \cdot v(\mathrm{CH_4}^R)}{4v_0(\mathrm{CH_4})} \cdot 100\ \%.$$

2.3.2. Methane dry reforming performance in steady-state conditions. Pretreatment before reaction was the same as in the case of CLMDR. The experiments were carried out in the temperature range of 600 – 750 °C, contact time was 10 ms. The initial mixture was 15 vol. % CH_4 + 15 vol. % CO_2 + balance N_2 following the earlier described procedure [20, 22].

3. Results and discussion

3.1. Textural and structural properties

Figure 1 shows XRD patterns for catalysts. Reflections corresponding to the cubic fluorite lattice CeO_2–ZrO_2 (PDF 81–0792) and NiO phase (PDF 47–1049) are observed.

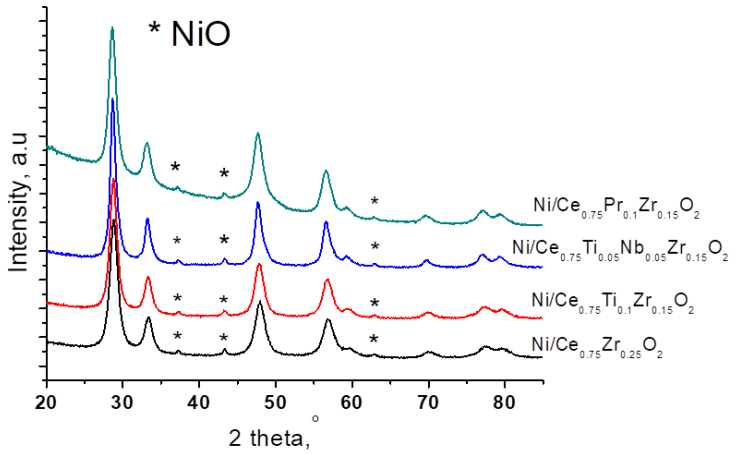

FIG. 1. XRD patterns of fresh catalysts

Table 1 shows specific surface area of studied catalysts and cell parameter and crystallite size of fluorite phase. The S_{BET} is close for three of studied catalysts, but is significantly lower for Pr-containing sample. The values of crystallite size of fluorite phase estimated from diffraction patterns are 9 – 14 nm. The crystallite size of NiO is between 20 – 30 nm for all samples. The change of cell parameter of ceria-zirconia fluorite phase after addition of Ti, Nb and Pr confirms incorporation of dopant cations into fluorite lattice.

A more detailed characterization of the samples is presented in our previous works, where the presence of oxygen vacancies in ceria-based catalysts prepared in supercritical isopropanol was shown based on XRD and Raman data [20, 21, 25].

The morphology of catalysts was studied by transmission electronic microscopy (TEM). The TEM images of fresh catalysts are presented in the Figure 2. Particles of fluorite phase have near-spherical shape with sizes about 15 – 20 nm and are packed into large ($\sim$ 100 nm) agglomerates [20, 25].

Nickel is presented on the support surface in the form of NiO particles, the corresponding interplanar distances are shown in the Fig. 2(b,d). NiO particles are also marked by blue circles in the Fig. 2(a,c). The particle size of NiO is about 10 – 20 nm for TiNb-doped sample and 20 – 30 nm for Pr-doped sample. It also should be noted, that NiO particles for Pr-containing sample have close to cubic shape, which, together with their larger size, also suggests their weak bound with the support.

TABLE 1. Surface area (BET) and fluorite crystallites size (from XRD) of the studied catalysts

Catalyst	S_{BET} (m^2/g)	$d_{fluorite}$ (nm)	d_{NiO} (nm)	Cell parameter of fluorite phase (Å)
$Ni/Ce_{0.75}Zr_{0.25}O_2$	21	9.4	30	5.368
$Ni/Ce_{0.75}Ti_{0.1}Zr_{0.15}O_2$	23	10.4	20	5.379
$Ni/Ce_{0.75}Ti_{0.05}Nb_{0.05}Zr_{0.15}O_2$	26	14.5	24	5.392
$Ni/Ce_{0.75}Pr_{0.1}Zr_{0.15}O_2$	9	11	23	5.394

The homogeneous distribution of support cations in all catalysts was shown by dark-field images with EDX analysis (Fig. 3).

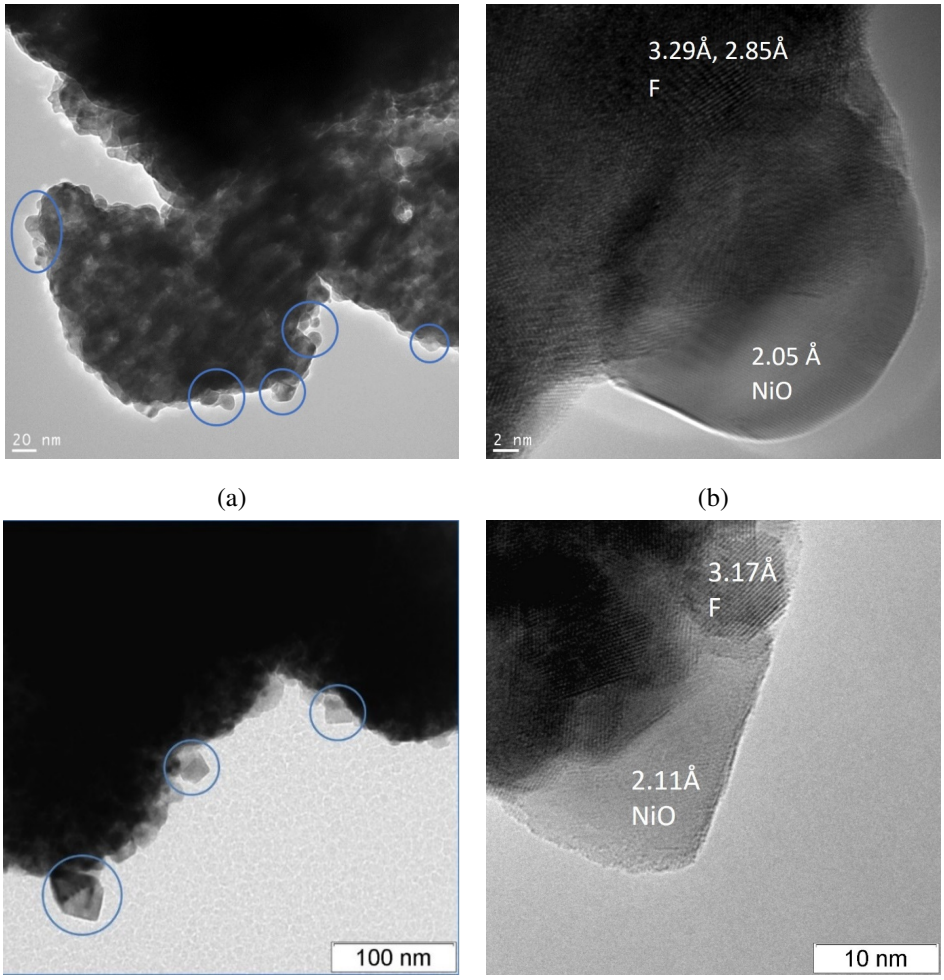

FIG. 2. TEM images of fresh catalysts $Ni/Ce_{0.75}Ti_{0.05}Nb_{0.05}Zr_{0.15}O_2$ (a,b [22]), $Ni/Ce_{0.75}Pr_{0.1}Zr_{0.15}O_2$ (c [25], d). F denotes the fluorite phase. NiO particles are marked by circles

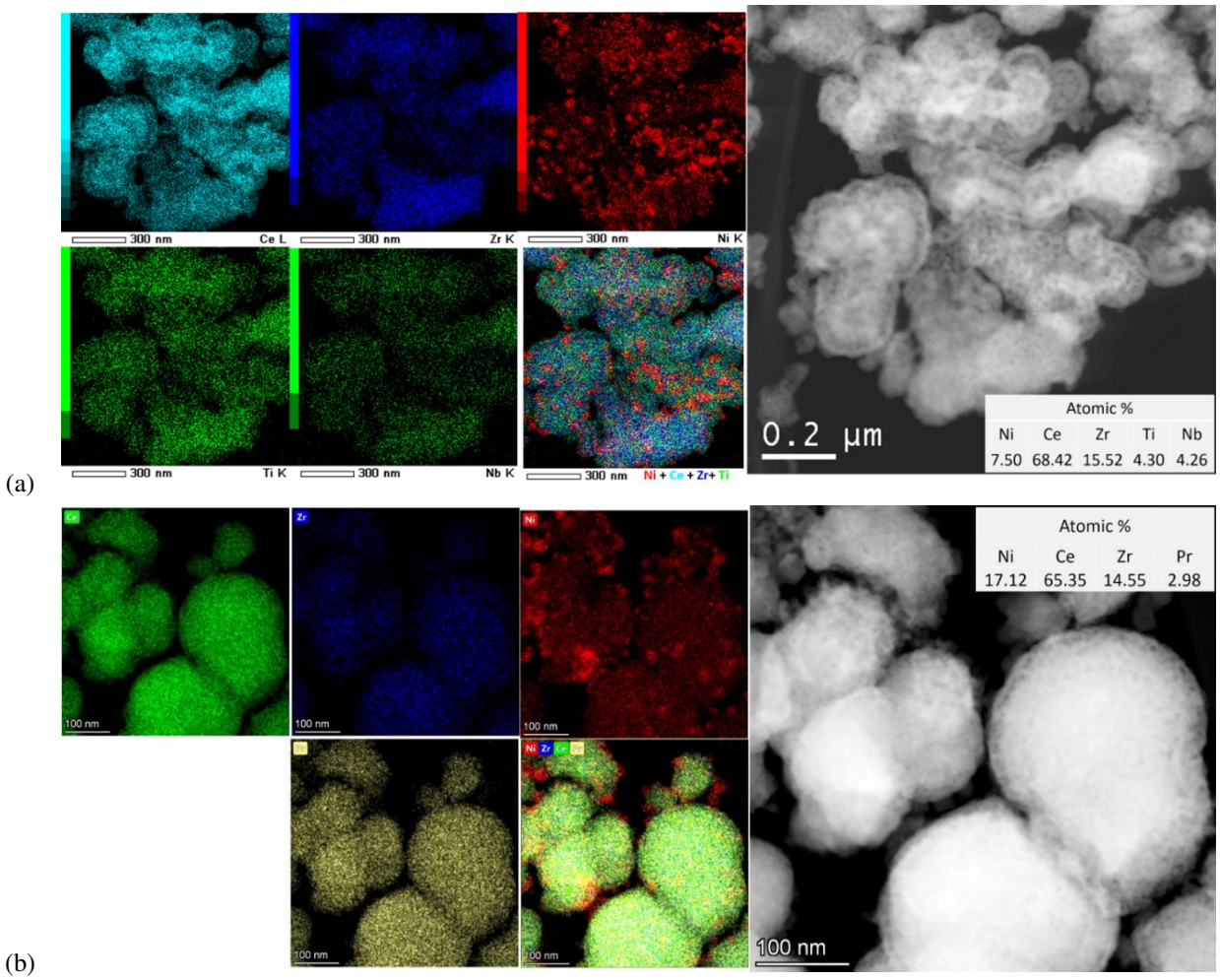

FIG. 3. HAADF-STEM images with EDX analysis of fresh catalysts a) $Ni/Ce_{0.75}Ti_{0.05}Nb_{0.05}Zr_{0.15}O_2$, b) $Ni/Ce_{0.75}Pr_{0.1}Zr_{0.15}O_2$

3.2. Catalysts reduction by H_2

Figure 4 shows H_2-TPR curves for supports and corresponding catalysts calcined at 700 °C [20, 25, 45]. For ceria, reduction peaks corresponding to removal of the surface/near-surface and bulk lattice oxygen are usually observed at 500 – 600 and 800 – 850 °C, respectively [46, 47].

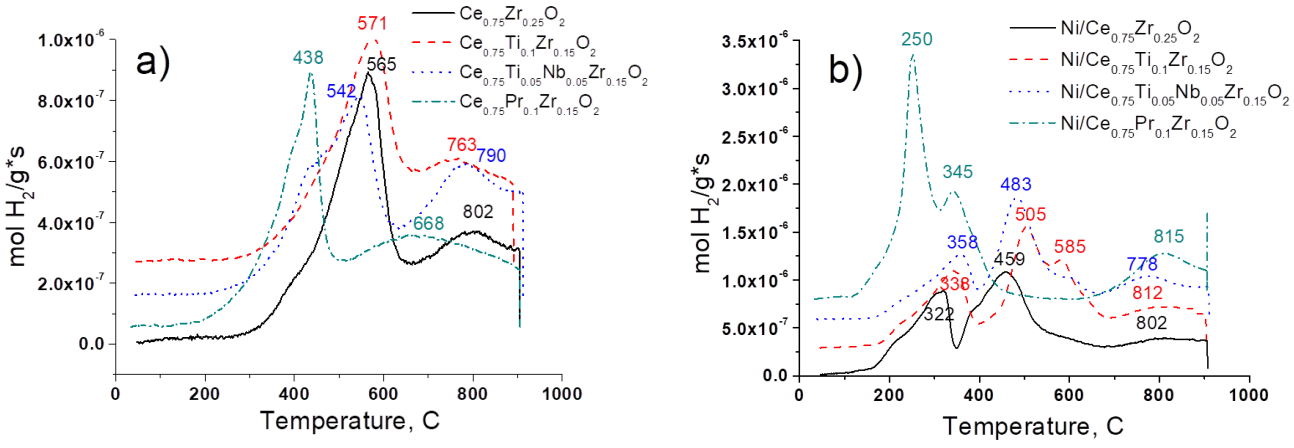

FIG. 4. H_2-TPR curves for supports (a) and corresponding catalysts (b) [20, 25]

It is worth noting, that the introduction of doping cations can promote the oxygen mobility and reactivity in modified CeO_2. For example, zirconium cations incorporated into ceria lead to reduction of the lattice oxygen at temperature below 800 °C [48]. In this work, the $Ce_{0.75}Zr_{0.25}O_2$ has peaks at 565 and 802 °C corresponding to reduction of the surface and bulk oxygen, respectively. The incorporation of Ti and Nb cations leads to a slight decrease of reduction temperatures compared with ceria-zirconia [20, 45]. At the same time, for Pr-doped sample, reduction peaks are shifted to lower temperatures by more than 100 °C which suggests its higher oxygen reactivity [25].

Amounts of hydrogen spent for the reduction of all samples are presented in the Table 2 and are quite close for all supports.

TABLE 2. H_2 consumption for studied supports and catalysts

	H_2 consumption, mmol/g_{cat}	
	Support	Ni/Support
$Ce_{0.75}Zr_{0.25}O_2$	1.36	2.21 [20]
$Ce_{0.75}Ti_{0.1}Zr_{0.15}O_2$	1.20	2.32 [20]
$Ce_{0.75}Ti_{0.05}Nb_{0.05}Zr_{0.15}O_2$	1.30	2.06 [20]
$Ce_{0.75}Pr_{0.1}Zr_{0.15}O_2$	1.21	2.14 [25]

The H_2-TPR reduction curves of the Ni-containing catalysts are presented in the Fig. 4(b). It is well known that metal-support interaction has very important role to red-ox properties of corresponding catalysts. This interaction can be very complex and results in presence of various forms of Ni species in the catalysts.

A weak shoulder at 200 °C corresponds to reduction of highly reactive oxygen surface species [49, 50]. For $Ni/Ce_{0.75}Zr_{0.25}O_2$ sample, there are two peaks in the region of middle temperatures, in contrast to one peak for the $Ce_{0.75}Zr_{0.25}O_2$ support. The first peak at 322 °C is due to the reduction of nickel oxide weakly interacting with support [51], while the second peak at 459 °C can be associated with the reduction of NiO particles strongly interacting with the oxide support [52].

Simultaneously with the reduction of nickel, the reduction of support cations also occurs [24, 45]. For Ti-containing catalysts, shift of these peaks to higher temperature is observed suggesting stronger interaction of supported Ni with oxide support [24].

For Pr-doped sample, on the contrary, reduction begins at lower temperature. In our earlier work [25], it was shown by XRD with *in situ* H_2 reduction, that peak at 250 °C can be attributed to reduction of active surface oxygen. Such shift for Ni-containing samples is associated with the facilitation of support reduction due to hydrogen spillover in the presence of nickel atoms [25]. The reduction of nickel also begins together with the support cations and finish at a lower temperature due to its weaker interaction with the support.

A more detailed characterization of TPR data can be found in our previous works [20, 25, 45].

3.3. Kinetic features of CLMDR

Figure 5(a) demonstrates the typical dependence of reagents and products concentration on reaction time at 700 °C using the $Ni/Ce_{0.75}Zr_{0.25}O_2$ catalyst as an example.

The catalyst reacts separately with methane and carbon dioxide at the reduction and oxidation stages, respectively.

It is assumed that several parallel processes occur at the reduction stage. First, the lattice oxygen interacts with CH_4 forming CO and H_2 by reaction of partial oxidation (7). The concentration of methane gradually increases, while the concentrations of H_2 and CO first increase to a maximum and then decrease due to limited amount of reactive oxygen of the catalyst.

$$CH_4 + [O] \rightarrow 2H_2 + CO^{R}. \tag{7}$$

Figure 6(a) presents data of H_2/CO^R ratio at reduction step. It is higher than 7 at the beginning of reaction and drops to 3 – 4 for last cycles which is still higher than 2 for partial oxidation (7). The formation of superstoichiometric H_2 can be explained by the occurrence of the second process, namely, the decomposition of methane according to reaction at (2). It can be seen that H_2/CO^R ratio decreases with the cycle number, so decrease in the contribution of methane decomposition reaction can be assumed.

Moreover, presence of a few amount of CO_2 at reduction stage indicates occurring reaction of complete oxidation of methane by highly reactive oxygen on the catalyst surface (8). Unfortunately, we have no information about formation of water because products concentration was measured by gas analyzer. However, both these products were observed at reduction step by Löfberg et al. [9].

$$CH_4 + 2[O] \rightarrow H_2O + CO_2^{R}. \tag{8}$$

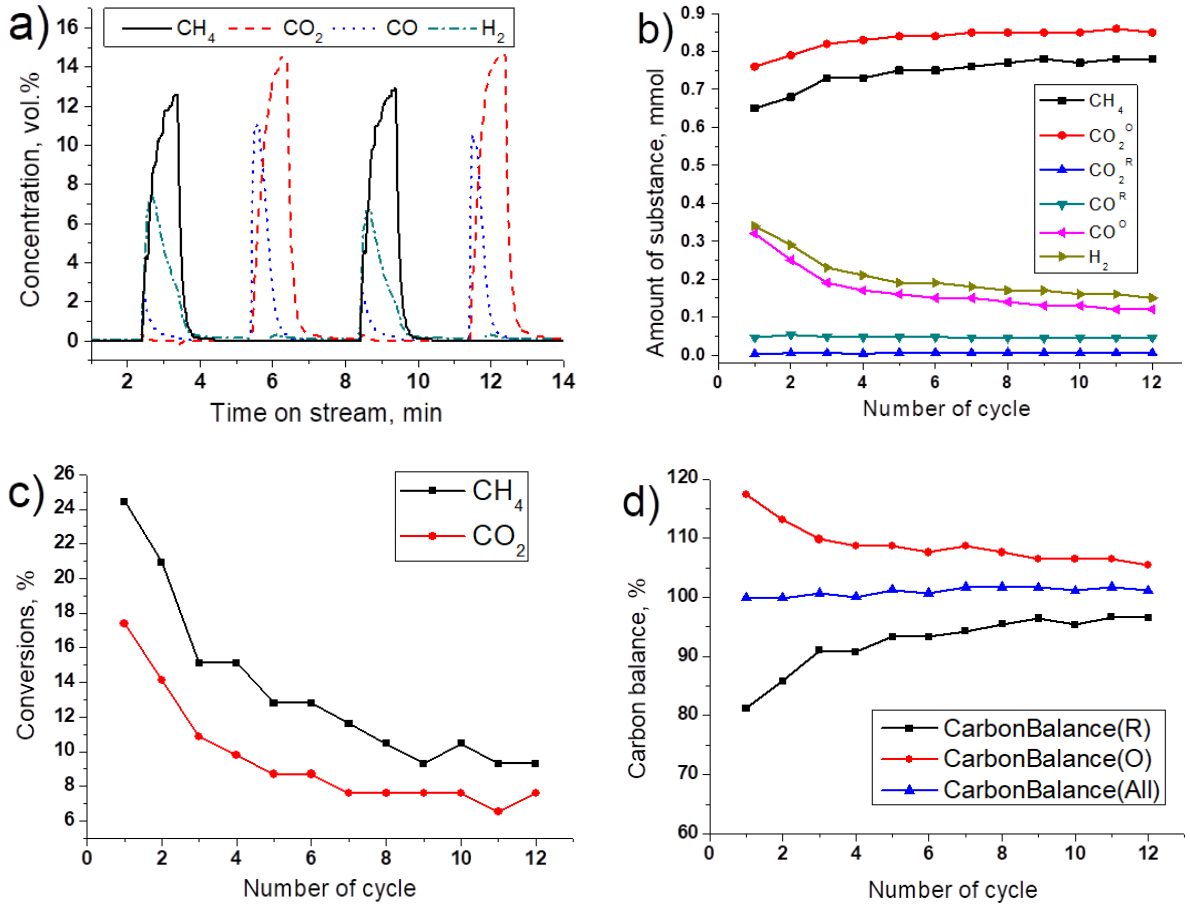

FIG. 5. Results of CLMDR experiment for Ni/$Ce_{0.75}Zr_{0.25}O_2$: a) the dependence of reagents and products concentrations on reaction time during 1st and 2nd cycles; b) the dependencies of CH_4, CO_2, CO, H_2 amounts on cycle number. CO^R/CO_2^R is CO/CO_2 produced at reduction step, CO^O/CO_2^O is CO/CO_2 produced at oxidation step; c) CH_4 and CO_2 conversions; d) carbon balances. Conditions: 15 vol.% CH_4 +15 vol.% CO_2 + 70 vol.% He, $T = 700\ ^\circ$C, $\tau = 10$ ms

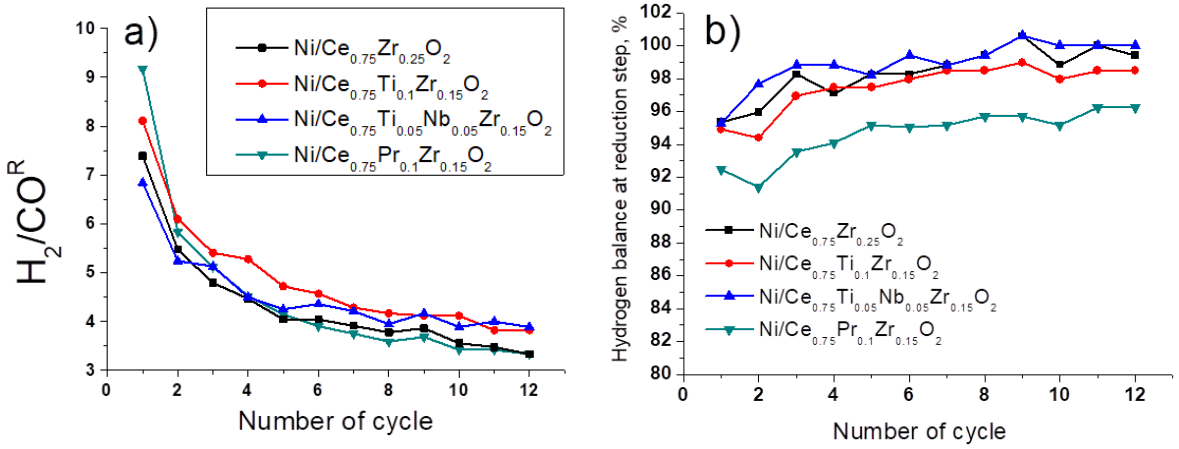

FIG. 6. a) The H_2/CO ratio at reduction step; b) hydrogen balance at reduction step

The hydrogen balances estimated at reduction step are presented in the Fig. 6(b). It can be seen that hydrogen balance is rather close to 100 % for the most of catalysts and is slightly lower for the Pr-doped sample. Based on the TPR data, it can be assumed that this sample contains more highly reactive oxygen, which leads to an increased oxidizing ability and lower hydrogen balance due to water formation.

Based on the data of CO_2 and CO formation at the reduction stage, the number of oxygen monolayers removed from the catalyst was calculated. It reaches $\sim 7 - 9$ monolayers for the Pr-containing sample and $\sim 3 - 4$ monolayers for other catalysts. So, this amount exceeds a monolayer even without taking into account the produced water, which indicates participation both of surface and lattice oxygen in the reaction process.

At the oxidation step there are also two routes of CO_2 consumption. The carbon generated by CH_4 decomposition can be oxidized by CO_2 forming CO (9). In addition, a negligible formation of hydrogen is observed, probably due to oxidation of CH_x species on the catalyst surface. The second parallel route of CO_2 consumption is oxidation of Ce_xO_y reduced species, during which the lattice oxygen consumed at the reduction stage is replenished (10). Another parallel route of CO_2 consumption, Ni oxidation by CO_2, is thermodynamically forbidden at the reaction temperature [8]. So, during oxidation stage, CO_2 conversion is gradually decreased due to replenishing of support oxygen and oxidation of carbon deposits.

$$CO_2 + C_{ads} \rightarrow 2CO^O, \tag{9}$$

$$CO_2 + [\,] \rightarrow CO^O + [O]. \tag{10}$$

Both of these processes lead to return of the catalyst to its initial oxidized state, which was before the reduction cycle, and the catalytic cycle is closed.

To some extent, this behavior is similar to that proposed for the red-ox Mars and Van Krevelen mechanism of such type reactions. It has been suggested that the mechanism of action of catalysts based on fluorites and perovskites with a high reactivity of lattice oxygen is of the red-ox type, and methane dry reforming proceeds with the participation of lattice oxygen [53]. In the present study, this assumption is also confirmed, since without the participation of lattice oxygen, the conversion of methane and CO_2 during the periodic supply of these reagents would be impossible.

3.4. Influence of the support composition on catalytic activity

One of the key tasks was to compare influence of doping cation on catalytic activity in CLMDR. In earlier investigations of our group, all these compositions were investigated in the conventional MDR [20, 22, 23, 45]. Catalysts doped by Pr and both Ti and Nb showed the highest activity due to their high defectiveness and presence of oxygen vacancies. So it was interesting how these features will affect the activity in CLMDR mode.

The dependencies of the substance amount of reagents and products on cycle number are presented in Fig. 5(b) using the example of $Ni/Ce_{0.75}Zr_{0.25}O_2$. Each point on the graphs is obtained by integrating the corresponding concentration curve at the stages of reduction or oxidation. The H_2 amount at oxidation step is not presented since it is close to zero. Based on these data, reagents conversions, products productivities and carbon balances were calculated.

Figures 5(c,d) presents reagents conversions and carbon balances for $Ni/Ce_{0.75}Zr_{0.25}O_2$ which are typical for all studied catalysts. It is known that CO_2 conversion is higher than CH_4 conversion in conventional MDR reaction because of influence of reverse water gas shift reaction (RWGS) [20]. However, in all cases in the present experiments in CLMDR, the values of CH_4 conversion are higher than CO_2 conversion that corresponds to decreasing influence of RWGS due to the separation of CO_2 and H_2 in time.

The features of carbon balances correspond to coke deposition at the reduction stage (< 100 %) with subsequent oxygenation of deposited carbon at oxidation stage (> 100 %). The carbon balance at the reduction stage in the first cycles is much lower, which, as was mentioned above, is due to higher contribution of the methane decomposition reaction. It should be taken into account that before the first cycle the catalyst is already in a reduced state with most of the support reactive oxygen being removed. Therefore, the contribution of the methane decomposition reaction is larger than that of the methane oxidation reaction.

The larger amount of carbon formed at the reduction step also leads to higher carbon balance at the oxidation step due to formation of additional CO from carbon deposits. It reaches 117 % and decreases with increasing cycle number. As a result, the total carbon balance at each cycle is close to 100 %.

For all studied catalysts, the similar behavior is shown (Fig. 7). The CH_4 and CO_2 conversions decrease from first cycles and reaches stationary values with an increase of the cycle number. The H_2 and CO productivities similarly decrease from 8 – 10 to 3 – 4 mmol/g.

Some differences are observed for the Pr-doped sample, for which, despite the highest methane conversion, lower H_2 and CO productivities are obtained. Since this sample also exhibits the lowest hydrogen and carbon (not shown) balances at the reduction stage, this may be due to loss of hydrogen in the form of water or CH_x species.

Another notable difference is the lowest CO_2 conversion for the TiNb-doped sample. This may be due to low methane conversion and high carbon balance at the reduction stage. So, for this sample, there is less deposited carbon, which can subsequently be oxidized at the oxidation stage, and less CO_2 is converted.

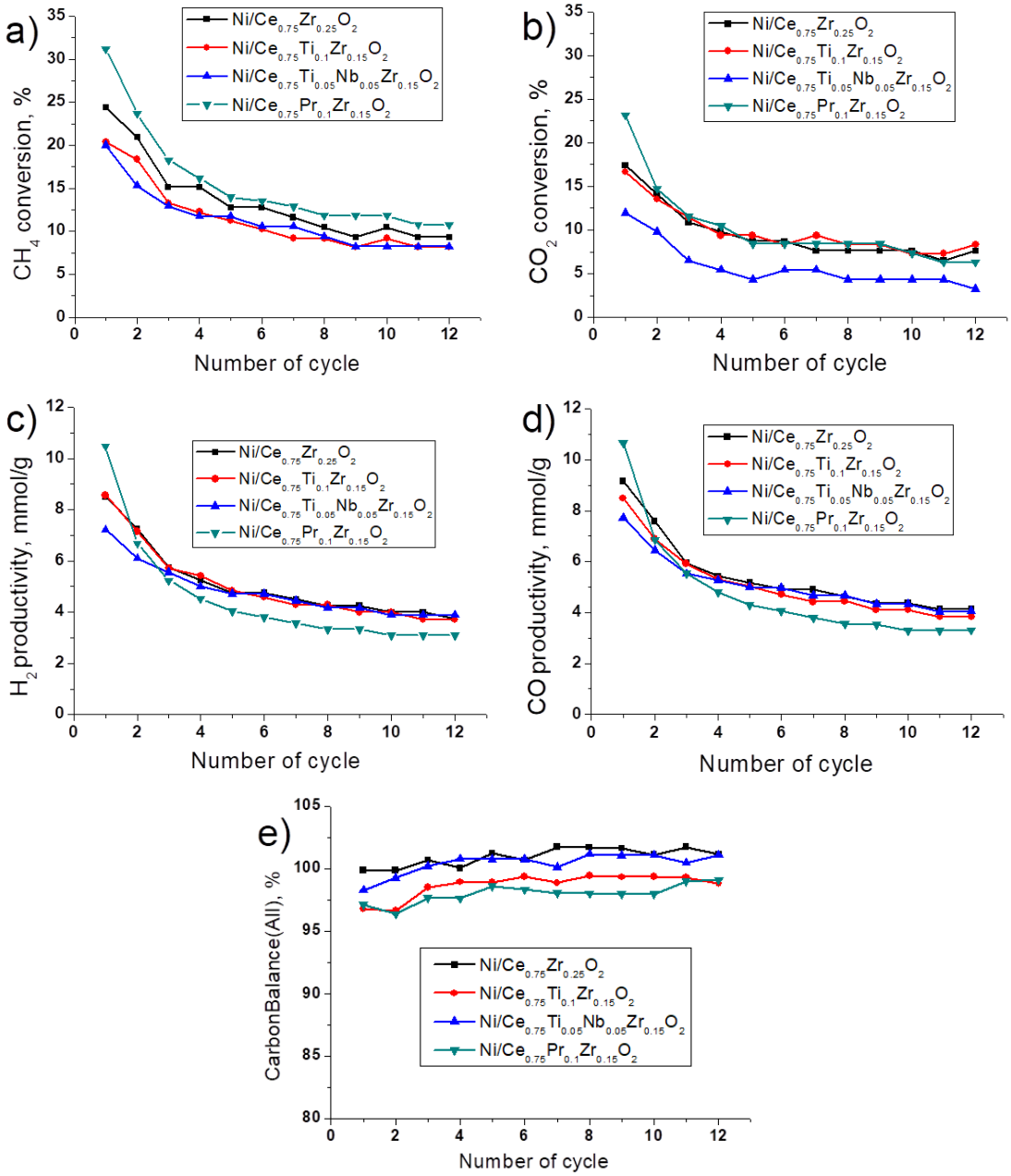

FIG. 7. The dependencies of CH_4 and CO_2 conversions (a,b), H_2 and CO productivities (c,d) and total carbon balances (e) on cycle number in CLMDR over studied catalysts

Catalysts after reaction were also investigated by HRTEM. Fig. 8 shows the micrographs for samples doped by TiNb (a) and Pr (b). There are metal nickel particles with sizes from 10 to 110 nm and small amounts of carbon fibers (not shown). However, there is no obvious difference in particle sizes depending on the composition of the oxide support.

To study the changes in catalyst structure at the oxidation stage, an additional *in situ* XRD experiment was carried out for $Ni/Ce_{0.75}Pr_{0.1}Zr_{0.15}O_2$ sample. A detailed description of the experiment is given in the experimental part. Fig. 9 shows the diffraction patterns and the lattice parameters of fluorite phase.

As was mentioned above, peaks of the fluorite and NiO phases are observed for the initial sample. After treatment in hydrogen, NiO is reduced to metallic nickel. The peaks of the fluorite phase shift towards smaller angles due to change in the lattice parameter, which increases from 5.4166 to 5.4892 Å. As was shown in [54], such increase is associated not only with the thermal expansion of the oxide crystal lattice, but also with the reduction of Ce^{4+} cations to Ce^{3+}.

After CO_2 supply, the lattice parameter decreases to 5.4599 Å as a result of the Ce^{3+} cations being oxidized back to Ce^{4+}. It is important to note that the formation of NiO does not occur. This is consistent with the results of thermodynamic calculations in [8], where it was shown that nickel is not oxidized by CO_2 at these temperatures. The second diffraction pattern under CO_2 stream was recorded after 2 hours later. During this time, the fluorite lattice parameter is further

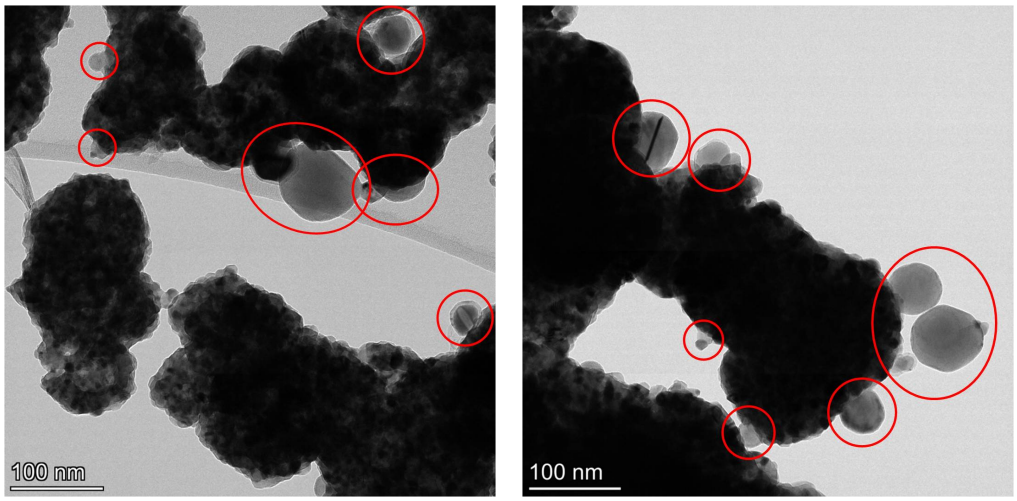

FIG. 8. TEM images of catalysts a) Ni/$Ce_{0.75}Ti_{0.05}Nb_{0.05}Zr_{0.15}O_2$; b) Ni/$Ce_{0.75}Pr_{0.1}Zr_{0.15}O_2$ after testing in CLDRM. Ni particles are marked by circles

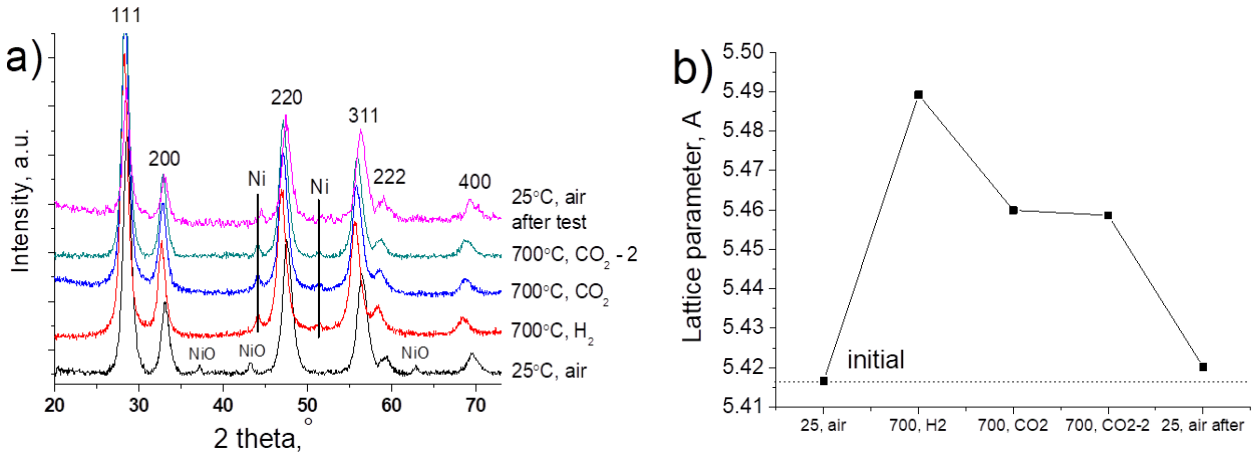

FIG. 9. Results of *in situ* XRD experiments on Ni/$Ce_{0.75}Pr_{0.1}Zr_{0.15}O_2$: a) diffraction patterns; b) dependence of lattice parameters of fluorite phase vs temperature

decreased to 5.4586 Å. Thus it can be concluded that the kinetics of support oxidation by CO_2 is quite slow [8]. However, this should not affect the catalytic activity, since the surface oxidation process is faster than the O diffusion in the bulk [55].

The last diffractogram was recorded after the sample was cooled in an inert environment and kept overnight in air. The lattice parameter is 5.4202 Å, which is slightly higher than the initial value and indicates a higher content of Ce^{3+} cations, so it can be concluded that complete oxidation of the oxide support to the initial state does not occur.

Thus, it was confirmed by *in situ* XRD that reduced oxide support is oxidized, while nickel remains in the metallic state under the CO_2 stream. Thus, even under conditions of CLMDR process, nickel particles remain in metallic form and only the support undergoes reduction and oxidation.

3.5. Comparison of MDR in steady-state condition and CLMDR

Detailed description of catalysts investigation in conventional steady-state MDR reaction is presented in our earlier works [20, 25] and will not be completely repeated here for the brevity. In general, the methane conversion at 700 °C decreases in the series Ni/$Ce_{0.75}Pr_{0.1}Zr_{0.15}O_2$ (50 %) > Ni/$Ce_{0.75}Ti_{0.05}Nb_{0.05}Zr_{0.15}O_2$ (44 %) > Ni/$Ce_{0.75}Zr_{0.25}O_2$ (35 %) > Ni/$Ce_{0.75}Ti_{0.1}Zr_{0.15}O_2$ (27 %). It is clear that the catalytic performance in the processes of CLMDR and MDR is not entirely correct to compare directly. However, it can be concluded, that carrying out reaction in the CLMDR mode for the studied samples eliminates the difference between various support compositions compared with conventional MDR process. Probably, it can be due to methane decomposition reaction, which occurs on metal nickel particles without participation of oxide support.

The ability of studied catalysts to conduct a cyclic process confirms our assumption that these catalysts with a high reactivity of oxygen implement a staged mechanism with independent stages of methane and CO_2 activation. The presence of reactive oxygen species makes it possible to separately feed the reagents, which leads to minimization of the influence

of RWGS side reaction. Indeed, if we compare the ratios of H_2 to total CO, it becomes clearly seen that these ratios on all catalysts are close to unity, being much higher than those in the course of the conventional MDR process (Fig. 10). If we take into account that in this study, the reduction step takes 1/6 of the cycle time and assume that the productivity by H_2 at the reduction stage tends to the value of 3 – 4 mmol·$g^{-1}h^{-1}$, then we can estimate some average performance, which will be about 0.5 – 0.7 mmol·$g^{-1}h^{-1}$. The productivity can be multiplied by using a two-reactor unit, in one reactor it is possible to carry out the reduction stage, in the other – the oxidation stage, alternately switching the oxidizer and reductant flows.

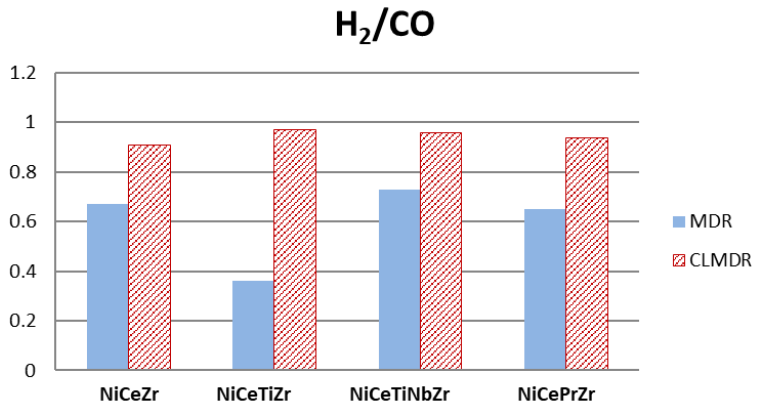

FIG. 10. The values of H_2/CO ratios for MDR and CLMDR (at the last cycle) processes. $T = 700\ ^\circ$C, $\tau = 10$ ms

4. Conclusions

The principle of chemical looping methane dry reforming reaction for Ni-containing catalysts based on modified ceria-zirconia was demonstrated. During the process, nickel remains in the form of metallic particles, and the support consistently participates in the processes of CH_4 oxidation and CO_2 reduction. Support modification has a weak effect on catalytic activity in CLMDR process compared with conventional MDR reaction. Using the CLMDR process, synthesis gas with a high H_2/CO ratio was obtained, which is acceptable for using as a feedstock for the production of hydrocarbons, which cannot be achieved on these catalysts with a conventional MDR process. The possibility of separating gas flows after the stage of oxidation and reduction can be used to obtain hydrogen-enriched gas for the needs of hydrogen energy.

References

[1] Wang Y., Yao L., Wang S., Mao D., Hu C. Low-temperature catalytic CO_2 dry reforming of methane on Ni-based catalysts: A review. *Fuel Process. Technol.*, 2018, **169**, P. 199–206.
[2] Manfro R.L., Souza M.M.V.M. Overview of Ni-Based Catalysts for Hydrogen Production from Biogas Reforming. *Catalysts*, 2023, **13**, 1296.
[3] Cai Y., Zhang Y., Zhang X., Wang Y., Zhao Y., Li G., Zhang G. Recent Advances in Ni-Based Catalysts for CH_4-CO_2 Reforming (2013–2023). *Atmosphere*, 2023, **14**, 1323.
[4] Zhang G., Liu J., Xu Y., Sun Y. A review of CH_4-CO_2 reforming to synthesis gas over Ni-based catalysts in recent years (2010–2017). *Int. J. Hydrogen Energy*, 2018, **43**, P. 15030–15054.
[5] Bradford M.C.J., Vannice M.A. CO_2 reforming of CH_4. *Catal. Rev.*, 1999, **41**, P. 1–42.
[6] Marinho A.L.A., Toniolo F.S., Noronha F.B., Epron F., Duprez D., Bion N. Highly active and stable Ni dispersed on mesoporous CeO_2–Al_2O_3 catalysts for production of syngas by dry reforming of methane. *Appl. Catal. B*, 2021, **281**, 119459.
[7] Li R., Zhang J., Shi J., Li K., Liu H., Zhu X. Regulation of metal-support interface of Ni/CeO_2 catalyst and the performance of low temperature chemical looping dry reforming of methane. *J. Fuel Chem. Technol.*, 2022, **50** (11), P. 1458–1470.
[8] Löfberg A., Guerrero-Caballero J., Kane T., Rubbens A., Jalowiecki-Duhame L. Ni/CeO_2 based catalysts as oxygen vectors for the chemical looping dry reforming of methane for syngas production. *Appl. Catal. B*, 2017, **212**, P. 159–174.
[9] Löfberg A., Kane T., Guerrero-Caballero J., Jalowiecki-Duhamel L. Chemical looping dry reforming of methane: towards shale-gas and biogas valorization. *Chem. Eng. Process.: Process Intensif.*, 2017, **122**, P. 523–529.
[10] Tang M., Xu L., Fan M. Progress in oxygen carrier development of methane-based chemical-looping reforming: A review. *Appl. Energy*, 2015, **151**, P. 143–156.
[11] Dawa T., Sajjadi B. Exploring the potential of perovskite structures for chemical looping technology: A state-of-the-art review. *Fuel Process. Technol.*, 2024, **253**, 108022.
[12] Zeng L., Cheng Z., Fan J.A., Fan L.-S., Gong J. Metal oxide redox chemistry for chemical looping processes. *Nat. Rev. Chem.*, 2018, **2**, P. 349–364.
[13] Kambolis A., Matralis H., Trovarelli A., Papadopoulou Ch. Ni/CeO_2–ZrO_2 catalysts for the dry reforming of methane. *Appl. Catal. A*, 2010, **377**, P. 16–26.
[14] Chen W., Zhao G., Xue Q., Chen L., Lu Y. High carbon-resistance Ni/$CeAlO_3$–Al_2O_3 catalyst for CH_4/CO_2 reforming. *Appl. Catal. B*, 2013, **136–137**, P. 260–268.
[15] Chen J., Wu Q., Zhang J., Zhang J. Effect of preparation methods on structure and performance of Ni/$Ce_{0.75}Zr_{0.25}O_2$ catalysts for CH_4–CO_2 reforming. *Fuel*, 2008, **87**, P. 2901–2907.

[16] Wu L., Xie X., Ren H., Gao X. A short review on nickel-based catalysts in dry reforming of methane: Influences of oxygen defects on anti-coking property. *Mater. Today Proc.*, 2021, **42** (1), P. 153–160.

[17] Safavinia B., Wang Y.M., Jiang C.Y., Roman C., Darapaneni P., Larriviere J., Cullen D.A., Dooley K.M., Dorman J.A. Enhancing $Ce_xZr_{1-x}O_2$ Activity for Methane Dry Reforming Using Subsurface Ni Dopants. *ACS Catal.*, 2020, **10** (7), P. 4070–4079.

[18] Pavlova S., Smirnova M., Bobin A., Cherepanova S., Kaichev V., Ishchenko A., Selivanova A., Rogov V., Roger A.-C., Sadykov V. Structural, Textural, and Catalytic Properties of Ni-$Ce_xZr_{1-x}O_2$ Catalysts for Methane Dry Reforming Prepared by Continuous Synthesis in Supercritical Isopropanol. *Energies*, 2020, **13**, 3728.

[19] Radlik M., Adamowska-Teyssier M., Krzton' A., Kozieł K., Krajewski W., Turek W., Costa P.D. Dry Reforming of methane over Ni/$Ce_{0.62}Zr_{0.38}O_2$ catalysts: Effect of Ni loading on the catalytic activity and on H_2/CO production. *C. R. Chim.*, 2015, **18**, P. 1242–1249.

[20] Simonov M., Bespalko Y., Smal E., Valeev K., Fedorova V., Krieger T., Sadykov V. Nickel-Containing Ceria-Zirconia Doped with Ti and Nb. Effect of Support Composition and Preparation Method on Catalytic Activity in Methane Dry Reforming. *Nanomaterials*, 2020, **10**, 1281.

[21] Bespalko Y., Smal E., Simonov M., Valeev K., Fedorova V., Krieger T., Cherepanova S., Ishchenko A., Rogov V., Sadykov V. Novel Ni/Ce(Ti)ZrO_2 Catalysts for Methane Dry Reforming Prepared in Supercritical Alcohol Media. *Energies*, 2020, **13**, 3365.

[22] Fedorova V., Simonov M., Valeev K., Bespalko Y., Smal E., Eremeev N., Sadovskaya E., Krieger T., Ishchenko A., Sadykov V. Kinetic Regularities of Methane Dry Reforming Reaction on Nickel-Containing Modified Ceria-Zirconia. *Energies*, 2021, **14**, 2973.

[23] Smal E., Bespalko Y., Arapova M., Fedorova V., Valeev K., Eremeev N., Sadovskaya E., Krieger T., Glazneva T., Sadykov V., et al. Carbon Formation during Methane Dry Reforming over Ni-Containing Ceria-Zirconia Catalysts. *Nanomaterials*, 2022, **12**, 3676.

[24] Smal E., Bespalko Y., Arapova M., Fedorova V., Valeev K., Eremeev N., Sadovskaya E., Krieger T., Glazneva T., Sadykov V., Simonov M. Dry Reforming of Methane over 5 % Ni/$Ce_{1-x}Ti_xO_2$ Catalysts Obtained via Synthesis in Supercritical Isopropanol. *Int. J. Mol. Sci.*, 2023, **24**, 9680.

[25] Arapova M., Smal E., Bespalko Y., Valeev K., Fedorova V., Hassan A., Bulavchenko O., Sadykov V., Simonov M. Methane Dry Reforming Catalysts Based on Pr-Doped Ceria-Zirconia Synthesized in Supercritical Propanol. *Energies*, 2023, **16**, 4729.

[26] Zagaynov I., Loktev A., Arashanova A., Ivanov V., Dedov A., Moiseev I. Ni(Co)-$Gd_{0.1}Ti_{0.1}Zr_{0.1}Ce_{0.7}O_2$ mesoporous materials in partial oxidation and dry reforming of methane into synthesis gas. *Chem. Eng. J.*, 2016, **290**, P. 193–200.

[27] Kim S.S., Lee S.M., Won J.M., Yang H.J., Hong S.C. Effect of Ce/Ti ratio on the catalytic activity and stability of Ni/CeO_2–TiO_2 catalyst for dry reforming of methane. *Chem. Eng. J.*, 2015, **280**, P. 433–440.

[28] Azevedo I.R., da Silva A.A.A., Xing Yu.T., Rabelo-Neto R.C., Luchters N.T.J., Fletcher J.C.Q., Noronha F.B., Mattos L.V. Long-term stability of Pt/$Ce_{0.8}Me_{0.2}O_{2-\gamma}$/$Al_2O_3$ (Me = Gd, Nb, Pr, and Zr) catalysts for steam reforming of methane. *Int. J. Hydrogen Energy*, 2022, **47**, P. 15624–15640.

[29] Wang Y., Zhang R., Yan B. Ni/$Ce_{0.9}Eu_{0.1}O_{1.95}$ with enhanced coke resistance for dry reforming of methane. *J. Catal.*, 2022, **407**, P. 77–89.

[30] Makri M.M., Vasiliades M.A., Petallidou K.C., Efstathiou A.M. Effect of support composition on the origin and reactivity of carbon formed during dry reforming of methane over 5 wt.% Ni/$Ce_{1-x}M_xO_2$-I (M = Zr^{4+}, Pr^{3+}) catalysts. *Catal. Today*, 2016, **259**, P. 150–164.

[31] Mastelaro V.R., Briois V., de Souza D.P.F., Silva C.L. Structural studies of a ZrO_2–CeO_2 doped system. *J. Eur. Ceram. Soc.*, 2003, **23**, P. 273–282.

[32] Kuznetsova T.G., Sadykov V.A., Moroz E.M., Trukhan S.N., Paukshtis E.A., Kolomiichuk V.N., Burgina E.B., Zaikovskii V.I., Fedotov M.A., Lunin V.V., Kemnitz E. Preparation of Ce–Zr–O composites by a polymerized complex method. *Stud. Surf. Sci. Catal.*, 2002, **143**, P. 659–667.

[33] Kambolis A., Matralis H., Trovarelli A., Papadopoulou Ch. Ni/CeO_2–ZrO_2 catalysts for the dry reforming of methane. *Appl. Catal. A*, 2010, **377**, P. 16–26.

[34] Montoya J.A., Romero-Pascual E., Gimon C., Del Angel P., Monzón A. Methane reforming with CO_2 over Ni/ZrO_2–CeO_2 catalysts prepared by sol-gel. *Catal. Today*, 2000, **63**, P. 71–85.

[35] Luisetto I., Tuti S., Romano C., Boaro M., Di Bartolomeo E., Kesavan J.K., Kumar S.S., Selvakumar K. Dry reforming of methane over Ni supported on doped CeO_2: New insight on the role of dopants for CO_2 activation. *J. CO_2 Util.*, 2019, **30**, P. 63–78.

[36] Hirano M., Hirai K. Effect of hydrolysis conditions on the direct formation of nanoparticles of ceria-zirconia solid solutions from acidic aqueous solutions. *J. Nanopart. Res.*, 2003, **5**, P. 147–156.

[37] Pradeep E., Habu T., Tooriyama H., Ohtani M., Kobiro K. Ultra-simple synthetic approach to the fabrication of CeO_2–ZrO_2 mixed nanoparticles into homogeneous, domain, and core-shell structures in mesoporous spherical morphologies using supercritical alcohols. *J. Supercrit. Fluids*, 2015, **97**, P. 217–223.

[38] Basile F., Mafessanti R., Fasolini A., Fornasari G., Lombardi E., Vaccari, A. Effect of synthetic method on CeZr support and catalytic activity of related Rh catalyst in the oxidative reforming reaction. *J. Eur. Ceram.*, 2019, **39**, P. 41–52.

[39] Manjunatha S., Dharmaprakash M.S. Thermal stability, optical and Photoluminescence properties of spherical $Ce_xZr_{1-x}O_2$ ($x = 0.05$) crystalline blue-emitting nanophosphors synthesized by microwave method. *Mater. Res. Express*, 2018, **5**, 035043.

[40] Guo J., Xin X., Zhang X., Zhang S. Ultrasonic-induced synthesis of high surface area colloids CeO_2–ZrO_2. *J. Nanopart. Res.*, 2009, **11**, P. 737–741.

[41] Khani Y., Bahadoran F., Shariatinia Z., Varmazyari M., Safari N. Synthesis of highly efficient and stable Ni/$Ce_xZr_{1-x}Gd_xO_4$ and Ni/X–Al_2O_3 (X = Ce, Zr, Gd, Ce–Zr–Gd) nanocatalysts applied in methane reforming reactions. *Ceram. Int.*, 2020, **46**, P. 25122–25135.

[42] Lovell E., Horlyck J., Scott J., Amal R. Flame spray pyrolysis-designed silica/ceria-zirconia supports for the carbon dioxide reforming of methane. *Appl. Catal.*, 2017, **546**, P. 47–57.

[43] Aymonier C., Loppinet-Serani A., Reveron H., Garrabos Y., Cansell F. Review of supercritical fluids in inorganic materials science. *J. Supercrit. Fluids*, 2006, **38**, P. 242–251.

[44] Tsybulya S.V., Cherepanova S.V., Soloviyova L.P. Polycrystal software package for IBM/PC. *J. Struct. Chem.*, 1996, **37** (2), P. 332–334.

[45] Arapova M., Smal E., Bespalko Yu., Fedorova V., Valeev K., Cherepanova S., Ischenko A., Sadykov V., Simonov M. Ethanol dry reforming over Ni supported on modified ceria-zirconia catalysts: the effect of Ti and Nb dopants. *Int. J. Hydrogen Energy*, 2021, **46**, P. 39236–39250.

[46] Luo M., Chen J., Chen L., Lu J., Feng Z., Li C. Structure and Redox Properties of CexTi1-xO2 Solid Solution. *Chem. Mater.*, 2001, **13**, P. 197–202.

[47] Zhu H., Qin Z., Shan W., Shen W., Wang J. Pd/CeO_2–TiO_2 catalyst for CO oxidation at low temperature: a TPR study with H_2 and CO as reducing agents. *J. Catal.*, 2004, **225**, P. 267–277.

[48] Kim J.R., Myeong W.J., Ihm S.K. Characteristics in oxygen storage capacity of ceria-zirconia mixed oxides prepared by continuous hydrothermal synthesis in supercritical water. *Appl. Catal. B*, 2007, **71**, P. 57–63.

[49] Ye J.L., Wang Y.Q., Liu Y., Wang H. Steam reforming of ethanol over Ni/$Ce_xTi_{1-x}O_2$ catalysts. *Int. J. Hydrogen Energy*, 2008, **33**, P. 6602–6611.

[50] Shan W., Luo M., Ying P., Shen W., Li C. Reduction property and catalytic activity of $Ce_{1-x}Ni_xO_2$ mixed oxide catalysts for CH_4 oxidation. *Appl. Catal. A*, 2003, **246**, P. 1–9.

[51] Montoya J.A., Romero-Pascual E., Gimon C., Del Angel P., Monzón A. Methane reforming with CO_2 over Ni/ZrO_2–CeO_2 catalysts prepared by sol-gel. *Catal. Today*, 2000, **63**, P. 71–85.

[52] Romero-Núñez A., Díaz G. High oxygen storage capacity and enhanced catalytic performance of NiO/$Ni_xCe_{1-x}O_{2-\delta}$ nanorods: Synergy between Ni-doping and 1D morphology. *RSC Adv.*, 2015, **5**, P. 54571–54579.

[53] Sadykov V., Rogov V., Ermakova E., Arendarsky D., Mezentseva N., Alikina G., Sazonova N., Bobin A., Pavlova S., Schuurman Y., Mirodatos C. Mechanism of CH_4 dry reforming by pulse microcalorimetry: metal nanoparticles on perovskite/fluorite supports with high oxygen mobility. *Thermochim. Acta*, 2013, **567**, P. 27–34.

[54] Pakharukova V.P., Potemkin D.I., Stonkus O.A., Kharchenko N.A., Saraev A.A., Gorlova A.M. Investigation of the Structure and Interface Features of Ni/$Ce_{1-x}Zr_xO_2$ Catalysts for CO and CO_2 Methanation. *J. Phys. Chem. C*, 2021, **125**, P. 20538–20550.

[55] Demoulin O., Navez M., Mugabo J.-L., Ruiz P. The oxidizing role of CO_2 at mild temperature on ceria-based catalysts. *Appl. Catal. B*, 2007, **70**, P. 284–293.

Submitted 3 June 2024; revised 10 October 2024; accepted 7 November 2024

Information about the authors:

Ekaterina Smal – Boreskov Institute of Catalysis SB RAS, 630090, Lavrentieva prospect, 5, Novosibirsk, Russia; ORCID 0000-0001-5068-8964; smal@catalysis.ru

Valeria Fedorova – Boreskov Institute of Catalysis SB RAS, 630090, Lavrentieva prospect, 5, Novosibirsk, Russia; ORCID 0000-0002-0551-1892; valeria@catalysis.ru

Konstantin Valeev – Boreskov Institute of Catalysis SB RAS, 630090, Lavrentieva prospect, 5, Novosibirsk, Russia; ORCID 0000-0001-5981-5018; valeev@catalysis.ru

Amir Hassan – Novosibirsk State University, 630090, Pirogova st., 1, Novosibirsk, Russia; ORCID 0000-0002-8725-186X; a.khassan1@g.nsu.ru

Evgeny Gerasimov – Boreskov Institute of Catalysis SB RAS, 630090, Lavrentieva prospect, 5, Novosibirsk, Russia; ORCID 0000-0002-3230-3335; gerasimov@catalysis.ru

Mikhail Simonov – Boreskov Institute of Catalysis SB RAS, 630090, Lavrentieva prospect, 5, Novosibirsk, Russia; ORCID 0000-0002-5161-5684; smike@catalysis.ru

Conflict of interest: the authors declare no conflict of interest.